Inorganic Chemistry

Article

pubs.acs.org/IC

Crystal Growth, Structural, Electrical, and Magnetic Properties of Mixed-Valent Compounds $YbOs_2Al_{10}$ and $LuOs_2Al_{10}$

Xu Zhang,[†,‡] Wei Yi,[§] Kai Feng,[⊥] Desheng Wu,[†] Yifeng Yang,[†] Ping Zheng,[†] Jiyong Yao,[⊥] Yoshitaka Matsushita,[¶] Akira Sato,[¶] Hongwei Jiang,[‡] Hai Wang,*[,‡] Youguo Shi,*[,†] Kazunari Yamaura,[∥] and Nanlin Wang[†]

[†]Beijing National Laboratory for Condensed Matter Physics & Institute of Physics, Chinese Academy of Sciences, Beijing 100190, China

[‡]Department of Physics, Capital Normal University, Beijing 100048, China

[§]International Center for Materials Nanoarchitectonics (WPI-MANA), National Institute for Materials Science, 1-1 Namiki, Tsukuba, Ibaraki 305-0044, Japan

[⊥]Center for Crystal Research and Development, Technical Institute of Physics and Chemistry, Chinese Academy of Sciences, Beijing 100190, China

[¶]Materials Analysis Station, National Institute for Materials Science, 1-2-1 Sengen, Tsukuba, Ibaraki 305-0047, Japan

[∥]Superconducting Properties Unit, National Institute for Materials Science, 1-1 Namiki, Tsukuba, Ibaraki 305-0044, Japan

Supporting Information

ABSTRACT: Single crystals of $YbOs_2Al_{10}$ and $LuOs_2Al_{10}$ were grown for the first time using an aluminum self-flux method. The compounds crystallized into a cagelike structure in space group *Cmcm*, similar to the prototype compound $YbFe_2Al_{10}$. $YbOs_2Al_{10}$ exhibited a mixed-valent nature, as determined by magnetic susceptibility measurements over a wide temperature range from 2 to 900 K, in which the inter−configuration−fluctuation model revealed a broad peak around 400 K. In contrast, $LuOs_2Al_{10}$ displayed Pauli-like paramagnetic behavior over the same temperature range. Both compounds were metallic in nature between 2 and 300 K. The electronic specific heat coefficient of 21.3(2) mJ mol^{-1} K^{-2} for $YbOs_2Al_{10}$ was determined to be larger than that for $LuOs_2Al_{10}$ [8.9(1) mJ mol^{-1} K^{-2}], reflecting the mixed-valent nature of the former. First-principles calculations predicted the presence of a mixed-valent state in $YbOs_2Al_{10}$, in agreement with the experimental observations. The novel compound $YbOs_2Al_{10}$ elucidates the evolution of the mixed-valent nature of the Yb-based ternary transition metal aluminides from the 3d to 5d elements.

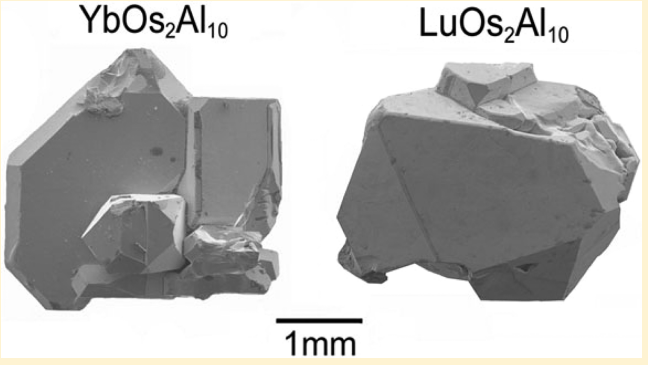

INTRODUCTION

Ternary rare earth (RE) transition metal (TM) aluminides are a large group of inorganic materials,[1] which possess characteristic physical properties such as Kondo semiconductivity, heavy Fermion behavior, unconventional superconductivity, and non-Fermi liquid conduction.[2−14] The exotic properties are usually rationalized as the interaction between localized 4f electrons and conduction electrons (c−f hybridization), as observed for Eu, Ce, and Yb-based compounds.[13] The hybridization often competes with other conduction electron phenomena such as the Rudermann−Kittel−Kasuya−Yoshida (RKKY) interaction.[15,16] Although the Doniach phase diagram resolved the quantum electromagnetic properties of this set of compounds,[17,18] it remains necessary to gather additional data on RE−TM−Al compounds for a more rounded understanding; the diagram helps to understand the fundamental aspects of correlated materials toward scientific and practical applications such as magnetocaloric materials, optical and magnetic devices, and thermoelectric materials.[2,3]

RE−TM−Al compounds usually crystallize into a so-called ordered binary structure as found in $YbFe_2Al_{10}$,[19] $CeRu_{3-x}Al_{10+x}$,[20] $Ce_2Ru_3Al_{15}$,[21] $Gd_3Ru_4Al_{12}$,[22] CeRuAl,[23] $La_{11}Ru_2Al_6$,[24] $La_5Ru_3Al_2$,[25] and Gd_4RhIn.[26] Furthermore, each compound has unique structural motifs, complicating the structures of the materials in this system. In terms of the general structural behavior of compounds of this type, $RETM_2Al_{10}$, $REFe_2Al_{10}$ (RE = Y, La−Nd, Sm, Gd−Lu), $RERu_2Al_{10}$ (Y, La−Nd, Sm, Gd, Tb, Ho−Yb),[26] $REOs_2Al_{10}$ (La−Nd, Sm, Gd),[27,28] and UTM_2Al_{10} (TM = Fe, Ru, Os)[29−31] adopt the prototypical $YbFe_2Al_{10}$ structure, which is an orthorhombic variant of the tetragonal $ThMn_{12}$ structure.[18]

Received: December 31, 2013
Published: April 21, 2014

   dx.doi.org/10.1021/ic403168v | *Inorg. Chem.* 2014, 53, 4387−4393

$REMn_2Al_{10}$ and $RERe_2Al_{10}$ (RE = Y, La−Nd, Sm, Gd−Dy, Yb) crystallize in either the $ThMn_{12}$- or $CaCr_2Al_{10}$-type structures.[32,33]

In recent years, $YbFe_2Al_{10}$-type compounds have captured considerable attention because $CeTM_2Al_{10}$ (TM = Fe, Ru, and Os) have shown remarkable c-f hybridization, resulting in valence-fluctuation behavior as well as Kondo-like behavior. In contrast, other $REFe_2Al_{10}$ compounds were found to be antiferromagnetic (RE = Sm−Tm) or paramagnetic (RE = Pr, Nd, and Yb).[34] $CeFe_2Al_{10}$ showed more pronounced Kondo-like behavior than $CeRu_2Al_{10}$ and $CeOs_2Al_{10}$. Moreover, $CeFe_2Al_{10}$ showed an absence of any peculiar phase transitions down to a temperature of 40 mK, while $CeRu_2Al_{10}$ and $CeOs_2Al_{10}$ exhibited phase transitions at 27.3 and 28.7 K, respectively;[35] $CeFe_2Al_{10}$ was argued to be an intermediate-valent material since the magnitude of magnetic susceptibility was half of those for the Ru and Os compounds.[35] In the $YbFe_2Al_{10}$-type series, the Ce-based derivatives solely established the mixed-valent nature over the 3d to 5d series. To draw a comprehensive picture of the $YbFe_2Al_{10}$-type series, the mixed-valent nature of additional compounds from the 3d to the 5d elements requires further investigation.

We focused our attention on the synthesis and characterization of Yb-based compounds containing 3d to 5d elements with the $YbFe_2Al_{10}$-type structure; the 3d compound $YbFe_2Al_{10}$ and 4d $YbRu_2Al_{10}$ have been studied for many years, while the 5d compound $YbOs_2Al_{10}$ remains unknown to the best of our knowledge. Regarding the ternary Yb−Os−Al system, only the compound $Yb_{7+x}Os_{12}Al_{61+y}$[36] is known most likely due to the difficulty of crystal growth in conditions which included the high vapor pressure of Yb. In the present study, we were successful in growing crystals of $YbOs_2Al_{10}$. Crystals of the novel compound $LuOs_2Al_{10}$ was grown as well. Characterization of the compounds by single-crystal X-ray diffraction, magnetic susceptibility, isothermal magnetization, specific heat, electrical resistivity measurements, and first-principles calculations revealed the nature of $YbOs_2Al_{10}$ and $LuOs_2Al_{10}$; we found that $YbOs_2Al_{10}$ exhibits pronounced mixed-valent magnetic features.

EXPERIMENTAL SECTION

$YbOs_2Al_{10}$ and $LuOs_2Al_{10}$ crystals were grown by self-flux methods. The starting materials Yb or Lu (ingot, 99.99%, Sinopharm Chemical Reagent Co., Ltd. Shanghai, China), Os (ingot, 99.99%, General Research Institute For Nonferrous Metals, Beijing, China), and Al (chunk, 99.999%, General Research Institute For Nonferrous Metals, Beijing, China) were mixed in a molar ratio of 1:2:30 in a glovebox filled by Ar; each mixture was placed in an alumina ampule, which was sealed in a tantalum (Ta) tube under Ar. The Ta tube was sealed in an evacuated quartz tube, followed by heating in a furnace from room temperature to 1150 °C over a period of 20 h; the tube was maintained at this temperature for 48 h, and then cooled to 850 °C at a rate of 2 °C/h. The tube was then inverted at 850 °C and quickly spun in a centrifuge to remove the excess Al. Crystals with approximate dimensions of 3 × 3 × 2 mm were obtained for each compound (see Figure 1); the crystals possessed mirrorlike flat surfaces and were robust in air. The chemical composition of each compound was analyzed by energy-dispersive X-ray (EDX) spectroscopy using a Hitachi S-4800 scanning electron microscope (SEM) at an accelerating voltage of 15 kV, with an accumulation time of 90 s. The EDX measurements at different locations on the crystal surfaces indicated that the average composition is stoichiometric—$YbOs_2Al_{10}$ and $LuOs_2Al_{10}$—within an instrumental accuracy of 1−2%.

Selected single crystals were studied by X-ray diffraction on a Bruker SMART APEX II diffractometer at 293(2) K using Mo Kα radiation (λ = 0.71073 Å). The SAINT+ and XPREP programs were used for data acquisition, extraction/reduction, and empirical absorption correction.[37] The crystal structure was refined by full-matrix least−squares fitting on F^2 using the SHELXL-97 program.[38] The static magnetic susceptibility (χ) of a single crystal of $YbOs_2Al_{10}$ (or $LuOs_2Al_{10}$) was measured on a Magnetic Property Measurement System (MPMS; Quantum Design, San Diego, USA) between 2 and 300 K in an applied magnetic field of 10 kOe under field-cooling (FC) and zero-field-cooling (ZFC) conditions. The χ of $YbOs_2Al_{10}$ at high temperature (ranging from 300 to 900 K) was measured in a Physical Properties Measurement System (PPMS, Quantum Design). The isothermal magnetization was measured in a MPMS between +50 kOe and −50 kOe at various temperatures between 2 and 300 K. An amount of collected crystals (25.1 mg in total) was used for the measurements. The magnetic susceptibility of a quartz sample holder was measured independently to subtract the holder contribution from the total magnetic data. The electrical resistivity (ρ) and specific heat (C_p) of the crystals were measured in PPMS. The ρ data were measured upon cooling from 300 to 2 K using a standard four-probe technique with a gauge current of 0.5 mA. Platinum wires and silver paste were used to make electrical contacts on each crystal. The C_p was measured by a thermal-relaxation method between 2 and 300 K in PPMS; approximately 15 mg of crystals of each compound were used for the C_p measurements. The electronic density of states (DOS) and band dispersions were calculated by the local-density approximation (LDA) method based on density functional theory.[39] The WIEN2K package, which is based on the highly precise full-potential linearized augmented-plane-wave method, was used in the calculations.[40]

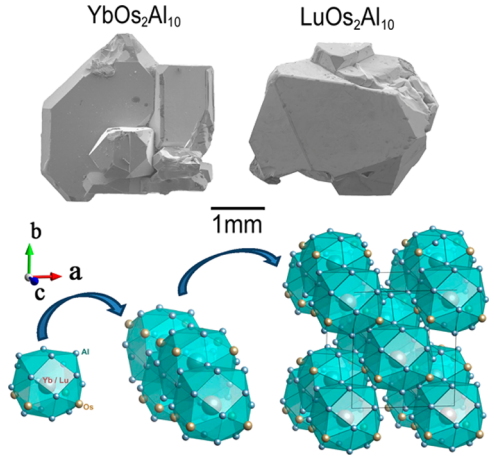

Figure 1. Structural view of cagelike orthorhombic $LnOs_2Al_{10}$.

RESULTS AND DISCUSSION

Reasonable structure refinement was achieved for the sets of single crystal X-ray diffraction data with the cagelike $YbFe_2Al_{10}$-type model,[19] which is orthorhombic, in space group *Cmcm*. The structural solutions for the compounds are summarized in Table 1; selected bond distances and angles are listed in Tables S1 and S2 in the Supporting Information. The *R* indices[38] were satisfactorily lower, indicating high quality of the refinements. Figure 1 illustrates the cagelike structure based on the present results; the polyhedral cage consists of Os and Al atoms with Yb (or Lu) atoms at the center. The polyhedra share edges in the *ac*-plane and corners along the *b*-axis with neighboring polyhedra.

We compare the lattice parameters of 5d $YbOs_2Al_{10}$ with those of the isostructural 3d $YbFe_2Al_{10}$ and 4d $YbRu_2Al_{10}$. Similarly to what was observed for $CeTM_2Al_{10}$ (TM = Fe, Ru, Os), the lattice parameters change little from 5d $YbOs_2Al_{10}$ [a = 9.1005(4) Å, b = 10.1855(4) Å, and c = 9.1118(5) Å] to 4d

dx.doi.org/10.1021/ic403168v | Inorg. Chem. 2014, 53, 4387−4393

Table 1. Crystallographic Data and Atomic Coordinates for $YbOs_2Al_{10}$ and $LuOs_2Al_{10}$

formula	$YbOs_2Al_{10}$	$LuOs_2Al_{10}$
molecular weight	823.24	825.17
temperature/K	293(2)	
wavelength	0.71073 Å (Mo Kα)	
space group	*Cmcm* (No. 63)	
lattice constants	a = 9.1005(4) Å	a = 9.0947(4) Å
	b = 10.1855(4) Å	b = 10.1608(5) Å
	c = 9.1118(5) Å	c = 9.1007(4) Å
unit cell volume	844.60(7) Å^3	840.99(7) Å^3
Z	4	
calculated density	6.4740 g/cm^3	6.517 g/cm^3
R-values	$R1$ = 2.88%, $wR2$ = 7.93%	$R1$ = 3.57%, $wR2$ = 9.04%
refinement software	SHELXL97	

atoms	Wyck.	x	y	z	U_{eq} (Å^2)
Os	8*d*	0.25	0.25	0	0.0041(3)
Yb	4*c*	0	0.372 76(5)	0.25	0.0069(3)
Al1	8*g*	0.3467 (3)	0.3696 (2)	0.25	0.0077(6)
Al2	8*f*	0	0.1241(3)	0.0452(4)	0.0094(6)
Al3	8*g*	0.2200(4)	0.1366(2)	0.25	0.0082(6)
Al4	8*f*	0	0.6554(3)	0.0997(3)	0.0073(5)
Al5	8*e*	0.2762 (6)	0	0	0.0078(9)
Os	8*d*	0.25	0.25	0	0.008 31(9)
Lu	4*c*	0	0.130 92(2)	0.25	0.011 73(9)
Al1	8*g*	0.3481(2)	0.132 03(15)	0.25	0.0116(3)
Al2	8*f*	0	0.376 45(15)	0.0461(2)	0.0128(3)
Al3	8*g*	0.2171(2)	0.364 68(15)	0.25	0.0123(3)
Al4	8*f*	0	0.154 31(17)	0.600 32(19)	0.0113(2)
Al5	8*e*	0.2245(3)	0	0	0.0123(3)

$YbRu_2Al_{10}$ [a = 9.0850(15) Å, b = 10.2150(15) Å, and c = 9.1110(15) Å],[26] but remarkably decrease to 3d $YbFe_2Al_{10}$ [a = 8.966(1) Å, b = 10.144(1) Å, and c = 8.993(2) Å].[19] As commonly observed for the $YbFe_2Al_{10}$-type compounds, a and c contract more than b from 5d to 3d across 4d. The anisotropy may reflect that the zigzag chains formed by the TM and Al bonds run along a and c axes. The structural anisotropy may result in anisotropic c-f hybridization as discussed for $YbTM_2Al_{10}$.[41]

The unit cell volume of $YbOs_2Al_{10}$ changes little (0.43%) than that of $LuOs_2Al_{10}$ [840.99(7) Å^3], regardless of the ionic radii of Yb and Lu, mostly likely because the Yb/Lu content in the unit cell is small (1/13). In addition, it is likely that the Al/Os cluster-like framework is rather rigid and hence the center atom (Yb/Lu) has a limited impact on the unit cell size. Alternatively, a mixed-valent nature of Yb of $YbOs_2Al_{10}$ has an impact on the volume change because that Eu-, Ce-, and Yb-based $RERu_2Al_{10}$ and $REFe_2Al_{10}$ showed a similar volume change beyond the lanthanide contraction, which was attributed to the mixed-valent nature.[27] We, however, unsuccessfully attempted to map out the unit-cell volume over the $REOs_2Al_{10}$ series; the limited number of available data did not allow its completion.

Figure 2 shows the temperature dependence of the magnetic susceptibility, χ, for both compounds of $YbOs_2Al_{10}$ and $LuOs_2Al_{10}$. The crystal direction was unfortunately unidentified because the unit cell parameters a, b, and c were too similar to identify the directions by Laue diffraction. Since the ZFC and FC curves were identical within instrumental accuracy over the temperature range, the ZFC curve accurately represented the relationship between χ and T. The χ versus T curve of $YbOs_2Al_{10}$ was rather complicated, as a broad peak appeared around 400 K, in addition to a sharp upturn at low temperatures. The broad peak is typical of mixed-valent Yb compounds, while the sharp upturn is unusual in Yb compounds;[4,42] this feature possibly reflects undetected magnetic impurities.

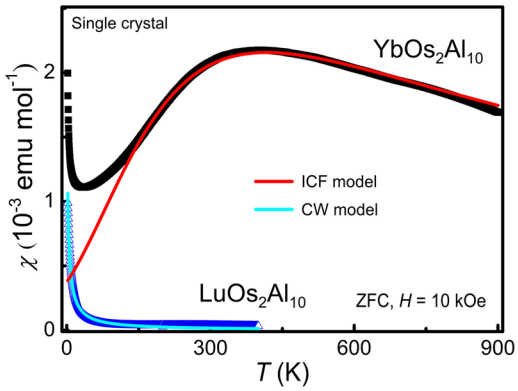

Figure 2. T dependence of χ for $YbOs_2Al_{10}$ and $LuOs_2Al_{10}$. Solid curves represent magnetic models to fit the data curves. Field-cooled (FC) curves are identical to the zero-field cooled (ZFC) curves.

It is known that the inter−configuration−fluctuation (ICF) concept has been developed to characterize the mixed-valent behavior of a compound; the magnetic data for $YbOs_2Al_{10}$ were therefore analyzed by the ICF model as $YbOs_2Al_{10}$ was magnetically analogous to the mixed-valent compounds $YbFe_2Al_{10}$ and $YbRu_2Al_{10}$.[43] The ICF model for Yb can be expressed by

dx.doi.org/10.1021/ic403168v | Inorg. Chem. 2014, 53, 4387−4393

$$\chi(T) = \frac{N_A(4.54\mu_B)^2 \upsilon(T)}{3k_B(T + T_{sf})} + \chi_0$$

where $\upsilon(T)$ is the fractional occupation of the Yb^{3+} state,

$$\upsilon(T) = \frac{8}{8 + \exp[-E_{ex}/k_B(T + T_{sf})]}$$

χ_0 is the temperature independent term, E_{ex} is the energy difference between the two valence states of Yb^{2+} and Yb^{3+}, and T_{sf} is the effective fluctuation temperature that characterizes the 4f electron energy level width. The electronic configuration of Yb^{3+} lies higher in energy level when $E_{ex} < 0$, and vice versa. Indicated by the solid curve in Figure 3a, the model

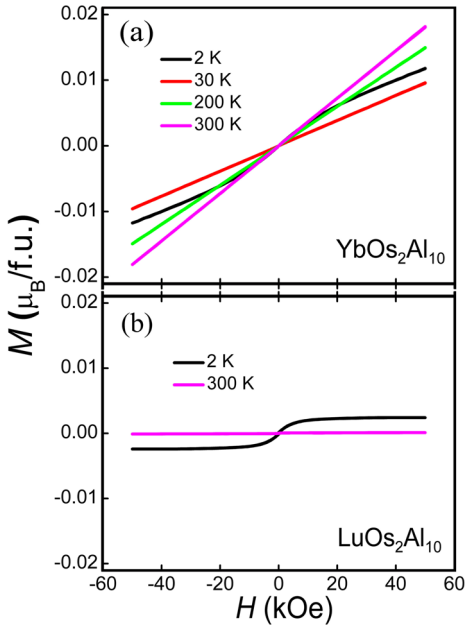

Figure 3. Isothermal magnetization of (a) $YbOs_2Al_{10}$ and (b) $LuOs_2Al_{10}$ as a function of temperature.

characterized the data well above 150 K, estimating the parameters of $E_{ex}/k_B = -1330(5)$ K, $T_{sf} = 220(1)$ K, and $\chi_0 = 1.4(2) \times 10^{-4}$ cm^3 mol^{-1}. The results indicate that the electronic configuration of Yb changes from the high energy level (Yb^{3+}, $4f^{13}$) to the low energy level (Yb^{2+}, $4f^{14}$) upon cooling, in good agreement with a mixed-valent hypothesis. In contrast, $LuOs_2Al_{10}$ showed a nearly temperature-independent χ without anomalies over the temperature range (Figure 2), implying Pauli-like paramagnetic behavior. The increase in χ of $LuOs_2Al_{10}$ at low temperature was well characterized by the Curie–Weiss model (see the solid curve). The analytical formula is $\chi = N_A\mu^2_{eff}/3k_B(T - \theta_p) + \chi_0$, where N_A is the Avogadro constant, μ_{eff} is the effective Bohr magneton, θ_p is the Weiss temperature, and k_B is the Boltzmann constant. The model fits the data well below 250 K, yielding $\theta_p = -2.5(3)$ K and $\mu_{eff} = 0.2(1)\ \mu_B$. The small magnetic moment indicated that the increase in χ was trivial. $LuOs_2Al_{10}$ is essentially paramagnetic, even at very low temperatures, consistent with the nonmagnetic picture of Lu^{3+}.[44]

$YbOs_2Al_{10}$ did not exhibit magnetic hysteresis between 2 and 300 K, where the magnetization evolved almost linearly with H (Figure 3a). The magnetization was far from saturation within the temperature and magnetic field ranges. The largest magnetization at 300 K and 50 kOe was just 0.018 μ_B/mol, corresponding to 0.4% of the full magnetization of Yb^{3+} (4.54 μ_B). The magnetic moment suggests that Yb^{2+} is dominant at 300 K and below. For comparison, the isothermal magnetization of $LuOs_2Al_{10}$ was measured in the same manner at 2 and 300 K, showing the absence of magnetic hysteresis and magnetization, which is consistent with the paramagnetic features of $LuOs_2Al_{10}$.

The C_p versus T curves for the compounds were well modeled by a combination of the Debye and Einstein models as indicated by the solid curves in Figures 4a and 4b.[45] No

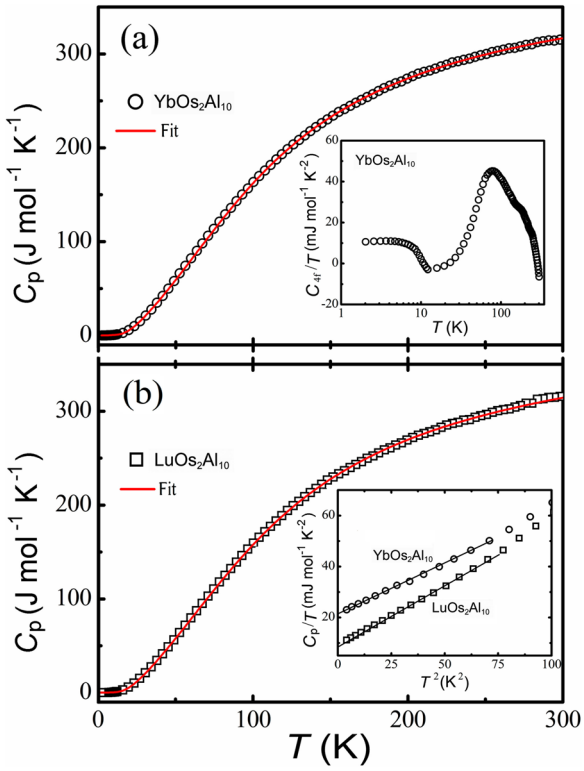

Figure 4. (a) C_p of $YbOs_2Al_{10}$ and (b) $LuOs_2Al_{10}$. The red solid curves represent fitting to a combination of the Debye and Einstein models. Inset to (a) shows the contribution of 4f electrons in $YbOs_2Al_{10}$; inset to (b) shows the C_p/T vs T^2 curves fit to a straight line.

anomalies representative of a phase transition (such as a peak and/or a hump) were detected, indicating the absence of phase transitions between 2 and 300 K. The high-temperature limit (300 K) of C_p was 316 J mol^{-1} K^{-1}, approaching to the Dulong–Petit limit $3nR$ (=324 J mol^{-1} K^{-1}), where n and R are the number of atoms per formula unit, and the molar gas constant, respectively.[46] In addition, the C_p/T versus T^2 curves at the low temperature limit ($T < 10$ K) for the compounds were well fit to the approximated Debye model $C/T = \gamma + 2.4\pi^4 nN_Ak_B(1/T_D^3)T^2$, where γ is the electronic term and T_D is the Debye temperature, as seen in the insets to Figure 4b. Analysis by the least–squares method yielded a γ value of 21.3(2) mJ mol^{-1} K^{-2} and a T_D of 396(5) K for $YbOs_2Al_{10}$; a γ of 8.9(1) mJ mol^{-1} K^{-2} and T_D of 377(2) K were obtained for $LuOs_2Al_{10}$. Compared with the γ of $YbTM_2Al_{10}$ (~75 and ~94 mJ mol^{-1} K^{-2} for TM = Fe[47] and Re,[48] respectively) and $CeOs_2Al_{10}$ (~514 mJ mol^{-1} K^{-2}),[49] the γ of $YbOs_2Al_{10}$ is significantly smaller. Even though, the γ of $YbOs_2Al_{10}$ is greater than that of $LuOs_2Al_{10}$, possibly reflecting the presence of a mixed-valent state of $YbOs_2Al_{10}$.[50,51]

dx.doi.org/10.1021/ic403168v | Inorg. Chem. 2014, 53, 4387–4393

The specific heat of the 4f electrons (C_{4f}) can roughly be estimated by subtracting the C_p of $LuOs_2Al_{10}$ from the C_p of $YbOs_2Al_{10}$. The subtracted data are presented in the inset to Figure 4a, in the form of a plot of C_{4f}/T versus T. A Schottky-like peak appears, as was observed for $CeFe_2Al_{10}$, which is typical for the hybridization-gap systems.[28,52] In addition, C_{4f}/T nearly saturates upon cooling below 10 K. The low-temperature upturn in the χ measurement is observed at the same temperature, suggesting a possible coupling between the C_{4f} and χ. If the coupling occurs around 10 K in $YbFe_2Al_{10}$, the low-temperature upturn of χ would probably be due to the c-f hybridization rather than undetected magnetic impurities. Further studies are required to clarify this issue.

The ρ of the compounds decreases monotonically upon cooling (Figure 5). The residual resistivity ratio, RRR ($=\rho_{300\ K}/\rho_{2K}$) was 21 and 26 for the Yb and Lu compounds, respectively. The RRR indicates the high quality of the crystals. Over the temperature range, the ρ of $YbOs_2Al_{10}$ is larger than that of $LuOs_2Al_{10}$, possibly because the magnetic moment of Yb has an impact on charge scattering. To quantitatively analyze the ρ versus T curve of $YbOs_2Al_{10}$ and $LuOs_2Al_{10}$, we applied the Fermi-liquid model $\rho(T) = \rho_0 + AT^2$, where ρ_0 and A are the residual resistivity and a constant, respectively,[51] to the curve below 25 K as shown in the inset to Figure 5. The model analysis yielded parameters ρ_0 of 16.2(4) $\mu\Omega$·cm and A of $5.1(1) \times 10^{-3}$ $\mu\Omega$·cm K^{-2} for $YbOs_2Al_{10}$, and ρ_0 of 5.01(4) $\mu\Omega$·cm and A of $1.85(8) \times 10^{-3}$ $\mu\Omega$·cm K^{-2} for $LuOs_2Al_{10}$, indicating Fermi-liquid-like behavior for both the compounds.[53]

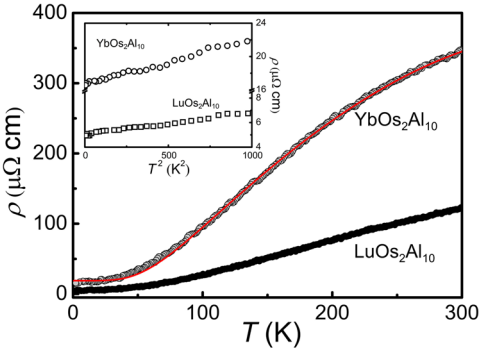

Figure 5. Temperature dependence of ρ of $YbOs_2Al_{10}$ and $LuOs_2Al_{10}$. The solid curve in red represents fitting to the Bloch–Grüneisen–Mott relation. (inset) Plot of ρ vs T^2 using the $YbOs_2Al_{10}$ and $LuOs_2Al_{10}$ data.

The ρ versus T curve of $YbOs_2Al_{10}$ was further analyzed over the whole temperature range by the Bloch–Grüneisen–Mott (BGM) model, which is expressed as

$$\rho(T) = \rho_0 + 4RT\left(\frac{T}{T_D}\right)^4 \int_0^{T_D/T} \frac{x^5 dx}{(e^x - 1)(1 - e^{-x})} - \alpha T^3$$

where R and α are constants, the second term represents contributions from the electron–phonon interaction, and the third term represents the s–d interband scattering.[54,55] The least-squares method resulted in fitting the data to the curve shown in Figure 5. The parameters were estimated to ρ_0 = 19(2) $\mu\Omega$ cm K^{-1}, R = 1.54(2) $\mu\Omega$ cm K^{-1}, T_D = 365(6) K, and $\alpha = 3.7(1) \times 10^{-6}$ $\mu\Omega$ cm K^{-3}. The T_D was slightly smaller than the 396 K derived from the low temperature C_p because the present T_D was averaged over the whole temperature range. The BGM analysis suggests that the s–d interband scattering is a significant factor in the charge transport.[28,31,56]

The electronic states of $YbOs_2Al_{10}$ and $LuOs_2Al_{10}$ were investigated theoretically by first-principles methods, as shown in Figure 6. The Os 5d and Al 3p orbitals hybridize to form the conduction bands in both the compounds. The spin–orbital splitting in the f-orbitals is approximately 1.5 eV; the Lu f-orbitals are fully occupied, whereas Yb has an intermediate valence close to 2.5 and its 4f orbitals hybridize with the conduction bands around the center of the Brillouin zone (red solid line). Consequently, the conduction bands are pushed upward by roughly 0.2 eV. The calculated DOS at E_F is 8.6 states eV^{-1} f.u.$^{-1}$ for $YbOs_2Al_{10}$ and 3.3 states eV^{-1} f.u.$^{-1}$ for

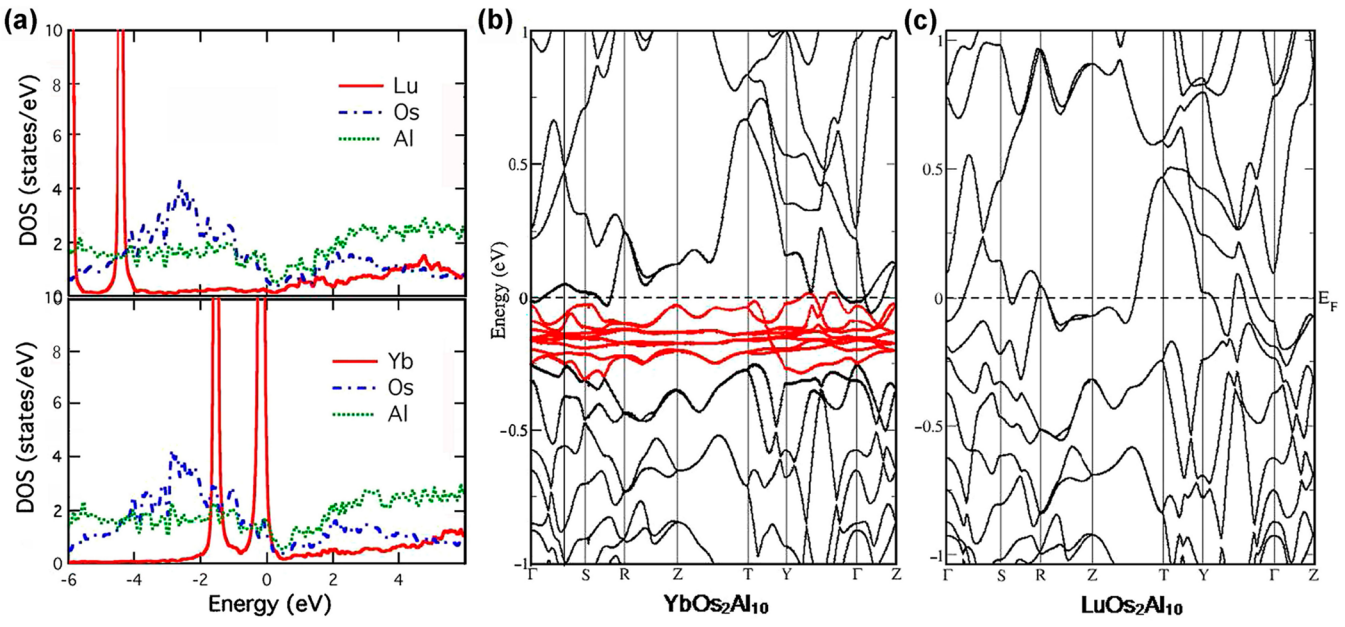

Figure 6. (a) LDA calculations for the electronic density of states, (b) the band dispersion of $YbOs_2Al_{10}$, and (c) $LuOs_2Al_{10}$.

dx.doi.org/10.1021/ic403168v | Inorg. Chem. 2014, 53, 4387–4393

$LuOs_2Al_{10}$, corresponding to γ = 20 mJ mol^{-1} K^{-2} and 7.8 mJ mol^{-1} K^{-2}, respectively. The theoretical γ for both compounds are in good agreement with the experimental results, implying that neither material is strongly correlated.

CONCLUSIONS

The novel 5d Os $YbOs_2Al_{10}$ is a continuation of the analogous $YbFe_2Al_{10}$ (3d) and $YbRu_2Al_{10}$ (4d) compounds in the Yb-based series; $YbOs_2Al_{10}$ therefore maps out the magnetic evolution over a 3d to 5d series in a similar manner to Ce-based systems.[28,52,57] The characterizing data obtained during this study reveals the mixed-valent nature of $YbOs_2Al_{10}$. The interatomic distances between the Yb and Os atoms in $YbOs_2Al_{10}$ may reflect the degree of hybridization between the 4f orbitals and conduction electrons;[28,52,57] the Yb−Os distance is 3.4538(2) Å, slightly longer than 3.4241 Å found in $YbFe_2Al_{10}$ and slightly shorter than 3.4606 Å observed in $YbRu_2Al_{10}$. The shorter distance implies a stronger hybridization, as was argued in studies of the Ce-based system. Further investigation of the relationship between the lattice and magnetic properties would be helpful to elucidate the role of the c-f hybridization in the Yb-based system; additional studies are currently underway in our laboratories.

Os-based $YbFe_2Al_{10}$-type compounds including $LaOs_2Al_{10}$, $PrOs_2Al_{10}$, $NdOs_2Al_{10}$, and $CeOs_2Al_{10}$ have been investigated;[27,28] however, a mixed-valent state has not yet been confirmed in such compounds. Surprisingly, the novel compound $YbOs_2Al_{10}$ synthesized in this study showed mixed-valent features. Because $YbOs_2Al_{10}$ does not manifest transitions with regard to a possible hybridization gap, the magnetic ground state of $YbOs_2Al_{10}$ is fundamentally distinct from that of $CeOs_2Al_{10}$;[6,58] further studies by inelastic neutron scattering may reveal the magnetic ground state of the Yb-based compounds and thus the essential nature of the mixed-valent state in moving from the 3d to the 5d series. The novel mixed-valent compound $YbOs_2Al_{10}$ develops Yb-based mixed-valent series as a counterpart of Ce-based mixed-valent series. These mixed-valent materials help to establish correlated electrons science that utilizes advanced materials technology.

ASSOCIATED CONTENT

Supporting Information

Selected bond distances and bond angles of $YbOs_2Al_{10}$ and $LuOs_2Al_{10}$, and details of the C_p data analysis. This material is available free of charge via the Internet at http://pubs.acs.org.

AUTHOR INFORMATION

Corresponding Authors

*E-mail: whseal@gmail.com. (H.W.)

*E-mail: ygshi@aphy.iphy.ac.cn. (Y.G.S.)

Notes

The authors declare no competing financial interest.

ACKNOWLEDGMENTS

We thank Prof. A. M. Strydom and Prof. P. J. Sun for physical properties discussion. This research was supported in part by the Ministry of Science and Technology of China (973 Project No. 2011CB921701 and 2011CBA00110), National Natural Science Foundation of China (No. 11274367, 11174339, 91122034), Chinese Academy of Sciences, the World Premier International Research Center of the Ministry of Education, Culture, Sports, Science, and Technology (MEXT) of Japan, the Japan Society for the Promotion of Science (JSPS) through a Grant-in-Aid for Scientific Research (25289233), and the Funding Program for World-Leading Innovative R&D on Science and Technology (FIRST Program), Japan.

REFERENCES

(1) Phelan, W. A.; Menard, M. C.; Kangas, M. J.; McCandless, G. T.; Drake, B. L.; Chan, J. Y. *Chem. Mater.* **2012**, *24*, 409−420.

(2) Haskel, D.; Lee, Y. B.; Harmon, B. N.; Islam, Z.; Lang, J. C.; Srajer, G.; Mudryk, Y.; Gschneidner, K. A., Jr.; Pecharsky, V. K. *Phys. Rev. Lett.* **2007**, *98*, 247205−1−247205−4.

(3) Sales, B. C.; Mandrus, D.; Williams, R. K. *Science* **1996**, *272*, 1325−1328.

(4) Cornelius, A. L.; Lawrence, J. M.; Ebihara, T.; Riseborough, P. S.; Booth, C. H.; Hundley, M. F.; Pagliuso, P. G.; Sarrao, J. L.; Thompson, J. D.; Jung, M. H.; Lacerda, A. H.; Kwei, G. H. *Phys. Rev. Lett.* **2002**, *88*, 117201−1−117201−4.

(5) Cho, B. K.; DiSalvo, F. J.; Kim, J. S.; Stewart, G. R.; Bud'ko, S. L. *Phys. B (Amsterdam, Neth.)* **1998**, *253*, 40−46.

(6) Kondo, A.; Wang, J. F.; Kindo, K.; Ogane, Y.; Kawamura, Y.; Tanimoto, S.; Nishioka, T.; Tanaka, D.; Tanida, H.; Sera, M. *Phys. Rev. B* **2011**, *83*, 180415(R)-1−180415(R)-4.

(7) Steglich, F.; Hellmann, P.; Thomas, S.; Gegenwart, P.; Link, A.; Helfrich, R.; Sparn, G.; Lang, M.; Geibel, C.; Assmus, W. *Phys. B (Amsterdam, Neth.)* **1997**, *237*, 192−196.

(8) Sereni, J. G. *J. Phys. Soc. Jpn.* **1998**, *67*, 1767−1775.

(9) Sereni, J. G.; Westerkamp, T.; Küchler, R.; Caroca-Canales, N.; Gegenwart, P.; Geibel, C. *Phys. Rev. B* **2007**, *75*, 024432−1−024432−8.

(10) Nakatsuji, S.; Kuga, K.; Machida, Y.; Tayama, T.; Sakakibara, T.; Karaki, Y.; Ishimoto, H.; Yonezawa, S.; Maeno, Y.; Pearson, E.; Lonzarich, G. G.; Balicas, L.; Lee, H.; Fisk, Z. *Nat. Phys.* **2008**, *4*, 603−607.

(11) Rojas, D. P.; FernándezBarquín, L.; Espeso, J. I.; Rodríguez Fernández, J.; Chaboy, J. *Phys. Rev. B* **2008**, *78*, 094412−1−094412−8.

(12) Trovarelli, O.; Geibel, C.; Mederle, S.; Langhammer, C.; Grosche, F. M.; Gegenwart, P.; Lang, M.; Sparn, G.; Steglich, F. *Phys. Rev. Lett.* **2000**, *85*, 626−629.

(13) Stewart, G. R. *Rev. Mod. Phys.* **2001**, *73*, 797−855.

(14) Park, K.; Wu, L. S.; Janssen, Y.; Kim, M. S.; Marques, C.; Aronson, M. C. *Phys. Rev. B* **2011**, *84*, 094425−1−094425−7.

(15) Subbarao, U.; Peter, S. C. *Inorg. Chem.* **2012**, *51*, 6326−6332.

(16) Aeppli, G.; Fisk, Z. *Comments Condens. Matter Phys.* **1992**, *16*, 155−170.

(17) Riseborough, P. S. *Adv. Phys.* **2000**, *49*, 257−230.

(18) Read, N.; Newns, D. M.; Doniach, S. *Phys. Rev. B* **1984**, *30*, 3841−3844.

(19) Niemann, S.; Jeitschko, W. *Z. Kristallogr.* **1995**, *210*, 338−341.

(20) Tursina, A. I.; Bukhan'ko, N. G.; Gribanov, A. V.; Noël, H.; Roisnel, T.; Seropegin, Y. D. *J. Alloys Compd.* **2005**, *400*, 194−196.

(21) Tursina, A. I.; Nesterenko, S. N.; Murashova, E. V.; Chernyshev, I. V.; Noël, H.; Seropegin, Y. D. *Acta Crystallogr., Sect. E: Struct. Rep. Online* **2004**, *E60*, i145−i146.

(22) Niemann, J.; Jeitschko, W. *Z. Anorg. Allg. Chem.* **2002**, *628*, 2549−2556.

(23) Hermes, W.; Matar, S. F.; Pöttgen, R. *Z. Naturforsch., B: Chem. Sci.* **2009**, *64b*, 901−908.

(24) Murashova, E. V.; Tursina, A. I.; Kurenbaeva, Z. M.; Noël, H.; Seropegin, Y. D. *Chem. Met. Alloys* **2010**, *3*, 101−107.

(25) Murashova, E. V.; Tursina, A. I.; Bukhanko, N. G.; Nesterenko, S. N.; Kurenbaeva, Z. M.; Seropegin, Y. D.; Noël, H.; Potel, M.; Roisnel, T.; Kaczorowski, D. *Mater. Res. Bull.* **2010**, *45*, 993−999.

(26) Tappe, F.; Schwickert, C.; Linsinger, S.; Pöttgen, R. *Monatsh. Chem.* **2011**, *142*, 1087−1095.

(27) Thiede, V. M. T.; Ebel, T.; Jeitschko, W. *J. Mater. Chem.* **1998**, *8*, 125−130.

(28) Muro, Y.; Kajino, J.; Onimaru, T.; Takabatake, T. *J. Phys. Soc. Jpn.* **2011**, *80*, SA021−1−SA021−3.

(29) Noël, H.; Goncalves, A. P.; Waerenborgh, J. C. *Intermetallics* **2004**, *12*, 189−194.
(30) Troc, R.; Pasturel, M.; Tougait, O.; Potel, M.; Noël, H. *Intermetallics* **2011**, *19*, 913−918.
(31) Sugai, T.; Haga, Y.; Matsuda, T. D.; Yamamoto, E.; Tateiwa, N.; Honda, F.; Settai, R.; Onuki, Y. *J. Phys.: Conf. Ser.* **2011**, *273*, 012122−1−012122−4.
(32) Thiede, V. M. T.; Jeitschko, W. *Z. Naturforsch., B: Chem. Sci.* **1998**, *53b*, 673−678.
(33) Fulfer, B. W.; Haldolaarachchige, N.; Young, D. P.; Chan, J. Y. *J. Solid. State Chem.* **2012**, *194*, 143−150.
(34) Morrison, G.; Haldolaarachchige, N.; Young, D. P.; Chan, J. Y. *J. Phys.: Condens. Matter* **2012**, *24*, 356002−1−356002−8.
(35) Nishioka, T.; Kawamura, Y.; Takesaka, T.; Kobayashi, R.; Kato, H.; Matsumura, M.; Kodama, K.; Matsubayashi, K.; Uwatoko, Y. *J. Phys. Soc. Jpn.* **2009**, *78*, 123705−1−123705−4.
(36) Niermann, J.; Jeitschko, W. *Inorg. Chem.* **2004**, *43*, 3264−3270.
(37) *SMART, SAINT+, and SADABS packages;* Bruker Analytical X-ray Systems Inc.: Madison, WI, 2002.
(38) Sheldrick, G. M. *SHELXL97 Program for the Solution and Refinement of Crystal Structures;* University of Göttingen: Germany, 1997.
(39) Hohenberg, P.; Kohn, W. *Phys. Rev.* **1964**, *136*, B864−B871.
(40) Blaha, P.; Schwarz, K.; Madsen, G. K. H.; Kvasnicka, D.; Luitz, J. *WIEN2K: An Augmented Plane Wave+Local orbitals Program for Calculating Crystal Properties;* Karlheinz Schwarz, Tech. Universitat Wien: Wien, Austria, 2001.
(41) Tanida, H.; Tanaka, D.; Sera, M.; Tanimoto, S.; Nishioka, T.; Matsumura, M.; Ogawa, M.; Moriyoshi, C.; Kuroiwa, Y.; Kim, J. E.; Tsuji, N.; Takata, M. *Phys. Rev. B* **2011**, *84*, 115128−1−115128−8.
(42) Mun, E. D.; Kwon, Y. S.; Jung, M. H. *Phys. Rev. B* **2003**, *67*, 033103−1−033103−3.
(43) Sales, B. C.; Wohlleben, D. K. *Phys. Rev. Lett.* **1975**, *35*, 1240−1244.
(44) Ohnishi, T.; Taniguchi, T.; Ikoshi, A.; Mizusaki, S.; Nagata, Y.; Lai, S. H.; Lan, M. D.; Noro, Y.; Ozawa, T. C.; Kindo, K.; Matsuo, A.; Takayanagi, S. *J. Alloys Compd.* **2010**, *506*, 27−32.
(45) Svoboda, P.; Javorský, P.; Diviš, M.; Sechovský, V.; Honda, F.; Oomi, G.; Menovsky, A. A. *Phys. Rev. B* **2001**, *63*, 212408−1−212408−4.
(46) Kittel, C. *Introduction to Solid State Physics,* 4th ed.; Wiley: New York, 1966.
(47) Khuntia, P.; Strydom, A.; Steglich, F.; Baenitz, M. *Phys. Status Solidi B* **2013**, *250*, 525−528.
(48) Sefat, A. S.; Bud'ko, S. L.; Canfield, P. C. *Phys. Rev. B* **2009**, *79*, 174429−1−174429−11.
(49) Lue, C. S.; Liu, H. F. *Phys. Rev. B* **2012**, *85*, 245116−1−245116−7.
(50) Hilscher, G.; Holland-Moritz, E.; Holubar, T.; Jostarndt, H. D.; Nekvasil, V.; Schaudy, G.; Walter, U.; Fillion, G. *Phys. Rev. B* **1994**, *49*, 535−550.
(51) Bauer, E. D.; Altarawneh, M. M.; Tobash, P. H.; Gofryk, K.; Ayala-Valenzuela, O. E.; Mitchell, J. N.; McDonald, R. D.; Mielke, C. H.; Ronning, F.; Griveau, J.; Colineau, E.; Eloirdi, R.; Caciuffo, R.; Scott, B. L.; Janka, O.; Kauzlarich, S. M.; Thompson, J. D. *J. Phys.: Condens. Matter* **2012**, *24*, 052206−1−052206−5.
(52) Yamashita, T.; Miyazaki, R.; Aoki, Y.; Ohara, S. *J. Phys. Soc. Jpn.* **2012**, *81*, 034705−1−034705−8.
(53) Senthil, T. *Phys. Rev. B* **2008**, *78*, 035103−1−035103−14.
(54) Mott, N. F. *Proc. R. Soc. London, Ser. A* **1936**, *153*, 699−717.
(55) Mott, N. F.; Jones, H. *The Theory of the Properties of Metals and Alloys;* Oxford University Press: London, U.K., 1958.
(56) Kangas, M. J.; Schmitt, D. C.; Sakai, A.; Nakatsuji, S.; Chan, J. Y. *J. Solid State Chem.* **2012**, *196*, 274−281.
(57) Strigari, F.; Willers, T.; Muro, Y.; Yutani, T.; Takabatake, T.; Hu, Z.; Agrestini, S.; Kuo, C.-Y.; Chin, Y.-Y.; Lin, H.-J.; Pi, T. W.; Chen, C. T.; Weschke, E.; Schierle, E.; Tanaka, A.; Haverkort, M. W.; Tjeng, L. H.; Severing, A. *Phys. Rev. B* **2013**, *87*, 125119−1−125119−6.
(58) Robert, J.; Mignot, J.-M.; André, G.; Nishioka, T.; Kobayashi, R.; Matsumura, M.; Tanida, H.; Tanaka, D.; Sera, M. *Phys. Rev. B* **2010**, *82*, 100404(R)-1−100404(R)-4.